Additive Manufacturing 47 (2021) 102348

Contents lists available at ScienceDirect

Additive Manufacturing

journal homepage: www.elsevier.com/locate/addma

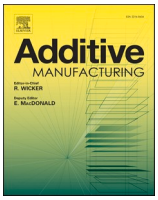

Research Paper

Direct writing of continuous carbon fibers/epoxy thermoset composites with high-strength and low energy-consumption

Zimeng Zhang [a,1], Ruochen Liu [b,1], Wei Li [a], Yuchen Liu [a], Haochen Luo [a], Li Zeng [a,2], Jingjing Qiu [c,*], Shiren Wang [a,b,**]

[a] Department of Industrial and Systems Engineering, Texas A&M University, College Station, TX 77843, USA
[b] Department of Materials Science and Engineering, Texas A&M University, College Station, TX 77843, USA
[c] Department of Mechanical Engineering, Texas Tech University, Lubbock, TX 77409, USA

ARTICLE INFO

Keywords:
Direct-Ink-Writing
Frontal polymerization
Additive manufacturing
Epoxy resin
Continuous carbon fiber composites
Thermosets
Low energy consumption

ABSTRACT

Epoxy resin-based thermoset composites are extensively used in industries with billions of dollars in revenue every year. High-rate manufacturing process is highly sought-after to produce complex composite structures with geometric flexibility and low energy-consumption. This work demonstrates printing and in-situ cure of epoxy resin-based thermosets and composites via self-sustaining frontal propagation. Specifically, latent initiator in the resin formulation was tuned from 2 mol% to 0.05 mol% to lower the frontal propagation temperature from ~290 °C to ~240 °C without decreasing the reaction rate. The epoxy resin was soaked into continuous carbon fiber (CF) tows and then printed through a modified direct ink writing system. Synchronization of the printing process and in-situ frontal curing resulted in continuous CF/thermoset composites (c-CFTC). Both single and dual nozzle print-heads were used to print c-CFTC with tunable fiber volume fractions. As-printed specimens exhibited exceptional tensile strength, 1.15 GPa at 48 vol% fibers and 0.42 GPa at 18 vol% fibers in fiber direction and ~35.5 MPa in transverse direction. The energy consumption of the printing process was also calculated, indicating 3.6 billion kilowatt-hours (kWh)/year energy-saving in comparison to conventional manufacturing processes with hours of high-temperature oven curing, equivalent to the energy consumption of 360,000 US families per year (single US family electric consumption: 10,000 kWh/year). The printing speed was 7.5–13.8 cm/min dependent on the fiber fraction, and thus the production rate was estimated to be 400–800 cm^3/hour. Such a high-rate and energy-saving approach could revolutionize the c-CFTC industry and aerospace, automobile, and marine industries with environmental and energy sustainability.

1. Introduction

Continuous fiber-reinforced thermoset composites, particularly continuous carbon fiber(CF)/thermoset composites(c-CFTC), demonstrate outstanding mechanical performance, chemical resistance, thermal resistance, and low density, and they are extensively used in aerospace [1,2], automotive [3], marine [4–6], electrical [7], and coating [8] industries. In comparison to the conventional composites manufacturing methods, such as hand lay-up [9], filament winding [10] and resin infusion (i.e. vacuum assisted resin transfer molding [11]) [12], emerging additive manufacturing (AM) attracts lots of attentions due to the design/manufacturing flexibility [13–18]. Although many efforts have been made in AM process of the continuous CF reinforced thermoplastic composites, the attempts in AM process of continuous CF/thermosetting composites are still limited compared to neat resin and discontinuous fiber composites [19]. Unlike thermoplastics, irreversible curing thermosetting polymers makes difficult to printing c-CFTC [20–22]. Wang et al. impregnated the continuous carbon fiber tows with epoxy resin and used them as a feedstock for printing, and subsequently solidified the constructs by post-curing [23]. Inspired by LOM, Parandoush et al. cut the prepreg sheets, layered up, and then bonded them together for composites structures [24]. Derived from the

* Corresponding author.
** Corresponding author at: Department of Industrial and Systems Engineering, Texas A&M University, College Station, TX 77843, USA.
E-mail addresses: Jenny.Qiu@ttu.edu (J. Qiu), s.wang@tamu.edu (S. Wang).
[1] These authors contributed equally to this work.
[2] Present address: School of Data Science City University of Hong Kong Kowloon Tong, Hong Kong.

https://doi.org/10.1016/j.addma.2021.102348
Received 17 June 2021; Received in revised form 18 September 2021; Accepted 19 September 2021
Available online 22 September 2021

material jetting process, Shi et al. also developed a dynamic capillary-driven approach that jetted epoxy resin onto continuous fiber tows for fiber wetting and impregnation and formed the structure with a localized heat supply [12]. More recently, He et al. reported a more general method to print continuous fiber/thermoset composites via shear stress-based extrusion [22,25,26].

Recent progress on frontal polymerization, a process in which the polymerization self-propagates through the feedstock with a transient initial heat source, provides a promising way of rapid and energy-efficient printing of thermosets composites [27]. White et al. have demonstrated a graceful method in rapid and energy-efficient manufacturing of dicyclopentadiene (DCPD)-based thermosetting composites using the metathesis reaction with the presence of a highly efficient ruthenium Grubbs'-type II (GC2) catalyst [28–31]. But such reaction cannot be extended to in-situ curing any other thermosetting polymers, such as epoxy resins, which demonstrate a broad range of industrial applications including coating, thermal/electrical insulation, adhesion [32,33]. It is reported that epoxy resins reached a USD 8 billion revenue in 2020 [34], 10 times higher than the USD 0.86 billion revenue for DCPD [34]. Because of the large portion of epoxy resins used in industrial applications, a significant amount of energy could be saved if a similar in-situ curing process can be developed for epoxy resin printing. Radical induced cationic frontal polymerization (RICFC) is a promising route for epoxy frontal curing in which enough exothermic energy is released rapidly with the introduction of Lewis acid generator for acid catalyzed reaction. In RICFC, the enhanced reaction rate is accredited to the highly reactive hydrogen protons from the Lewis acid that protonate surrounding epoxides for nucleophile attacking. Weaker counterion nucleophilicity is preferred to provide higher reactivity and prevent early protonated epoxide termination to sustain the reaction front. Mariani et al. [35] and Bomze et al. [36] presented successful frontal curing of bisphenol-A-diglycidylether (BADGE) using SbF_6^--based iodonium salt (p-octyloxyphenyl)phenyliodonium hexafluoroantimonate (denoted as I-Sb) as cationic initiator and thermo-labile compounds 1,1,2,2-tetraphenyl-1,2-ethanediol (TPED) as a radical thermal initiator (I-TI). Such reaction obtained a relatively low front velocity of 2.7 cm/min[36], only 1/3 of DCPD front velocity, and a high front temperature exceeding 280 °C. The epoxy resins are not properly cured and turned scarlet or even black after curing because of the high reaction temperature. More recently, fluorinated alkoxyaluminate anion based iodonium salt (I-Al) was found to be a more efficient counterion for BADGE cationic curing and observed enhanced front velocity three times higher than I-Sb salt [37,38]. With such development in reaction, recently, Uitz et al. studied the process of neat epoxy resin printing via frontal polymerization in DIW [39]. However, the frontal curing enabled printing of high-performance c-CFTC has not been reported yet. The challenges lie in the process design with the presence of continuous fiber tows, as well as understanding the reaction kinetics for controllable printing.

In this article, we report frontal curing-enabled printing of continuous carbon fiber/epoxy thermoset composites with exceptional mechanical properties and low energy-consumption. Specifically, the continuous carbon fiber tows were soaked with frontal curable Bisphenol A diglycidyl ether (BADGE) epoxy resin, which is incorporated with highly efficient curing agents, fluorinated alkoxy aluminate (p-octyloxyphenyl) phenyliodonium salt (denoted as I-Al, used as cationic initiator) and thermo-labile compounds TPED (used as thermal initiator). As-wetted continuous carbon fiber tows were subsequently subjected to layer-by-layer deposition with self-propagating in-situ curing, resulting in a freestanding 3D structure defined by the computer model. The printing behavior and mechanical properties were analyzed.

2. Materials and methods

2.1. Materials

EPON 828, a commercialized BADGE based epoxy resin, was selected in this study. EPON 828 and amine-based curing agent 3300 were kindly provided by Hexion. Thermal initiator 1,1,2,2–tetraphenyl-1,2–ethandiol (TPED, noted as I-TI) was purchased from Sigma Aldrich. Cationic photoinitiator (p-octyloxyphenyl)phenyliodonium hexafluoroantimonate (noted as: I-Sb) was purchased from Alfa chemistry, and bis[4-(tert-butyl)phenyl]iodonium Tetra(nonafluoro-tert-butoxy) aluminate (noted as: I-Al) was purchased from TCI America. Dichloromethane (DCM) was purchased from Sigma Aldrich. Continuous carbon fiber tow used in this study was purchased from Hexcel company with the brand of HexTow Carbon Fiber 1M10-GS 12 K.

2.2. Frontal curable epoxy resin preparation

I-Al and I-TI were dissolved in DCM before mixing with epoxy resin. Different initiator concentrations of I-Al/I-TI ranging from 0.02 mol% −1 mol%/ 2 mol% −8 mol% to epoxy resin were prepared. The I-Al, I-TI, epoxy resin and DCM mixture were bath sonicated to ensure they are fully mixed. Then, the mixture was undergoing rotary evaporation to remove the solvent before printing.

2.3. Frontal curing assisted printing of epoxy resin

The reactive epoxy resin was prepared and loaded into the cartridge, then underwent the extrusion-based printing process for 3D construction. A pneumatic pressure-driven Allevi 1 3D bioprinter was used for printing with a thermocouple inserted print-bed for frontal propagation initiation. The print bed was set to 100–150 °C for initiation depending on different initiator concentrations. The cartridge was kept at room temperature. The resins cured in a few seconds upon extruded onto the print-bed. Subsequently, frontal curing propagated along the extruded resin, following the extruder and form the structure with the movement of the extruder in 3D space.

2.4. Front velocity and front temperature analysis

A non-destructive analysis (NDA) was used for measuring frontal velocity and frontal temperature of the frontal curing and printing process. Forward-looking infrared camera (FLIR A325sc) was installed to record the temperature profile of the printed filament at each time interval during the printing process. Thermal images was captured and used for processing frontal velocity and frontal temperature. Detailed analysis with specific examples was described in Fig. S3 and Note 2. Besides, a digital camera was employed to record the printing process. The IR camera was calibrated and compared with the temperature measured by the thermocouple (Fig. S4 and Note 2).

2.5. Heat of reaction, reaction kinetics, and thermal degradation measurements

Differential scanning calorimetry (DSC) measurements were employed on a DSC (Q20, TA Instruments) equipped with a CFL-50 cooling system. The measurements were performed in the temperature range of 50 °C −220 °C at a ramping rate of 20 °C/min with the Nitrogen flow rate of 50 mL/min. The reaction enthalpy is calculated by the total area of heat flow after baseline correction. Thermal degradation measurement was conducted on a thermogravimetric analysis (TGA) (Q50, TA Instruments) machine in air. Specimens were heated from room temperature to 600 °C at a ramping rate of 10 °C/min.

2.6. Neat epoxy sample fabrication

ASTM Type V tensile bars were fabricated. Tensile bars with different I-TI/I-Al molar ratios were printed. Conventionally oven cured (at 120 °C for 4 h) and bulk frontally cured tensile bars with 4 mol% I-TI and 0.05 mol% I-Al as control specimens. Besides, conventionally oven cured (at 120 °C for 4 h) tensile bars with a stochiometric amine-based curing agent (Epikure Curing Agent 3300) were prepared. For conventionally cured specimens, resins were poured into a PTFE mold and degassed under the vacuum to remove voids and bubbles.

2.7. Continuous CFTC Printing

Continuous carbon fiber composites were printed with either single nozzle or a self-modified coaxial nozzle to control the fiber/epoxy ratio of printed composites. The single and dual nozzle printing setups are illustrated in Fig. 1a and b, respectively. For both single and dual nozzle printing, the continuous carbon fiber tow was immersed in the reactive resin reservoir for impregnation. To initiate the curing reaction, a flexible heating unit (New Era, 33 W, 2 thermocouple, 90 cm cord, 1.5 cm x 50cm flat to spiral heating pad) was adhered onto the build platform and under the aluminum foil to adjust print bed temperature, as shown in Fig. 1c and d. The print bed temperature was set to 120 °C to initiate the frontal reaction. After initialized with a 10–20 s heating, the curing reaction starts and continues autonomously along with extruding strand, resulting in the in-situ solidified structure as defined by the computer model. To prevent clogging, an offset distance between the nozzle and the build layer was set to ~1 mm.

In single-nozzle extrusion captured in Fig. 1c and e, fiber tow was threaded into the print head before reactive resins were loaded into the syringe. Then the fiber tow was dragged out with resin coated when printing started. The nozzle size of 18 G was selected to accommodate the size of the continuous carbon fiber tows. Single nozzle printing is typical in 3D printing. For single nozzle printing, the nozzle inner diameter should be similar to the size of the fiber tows, and thus difficult to tune the resin amount. The filament was also difficult to move around

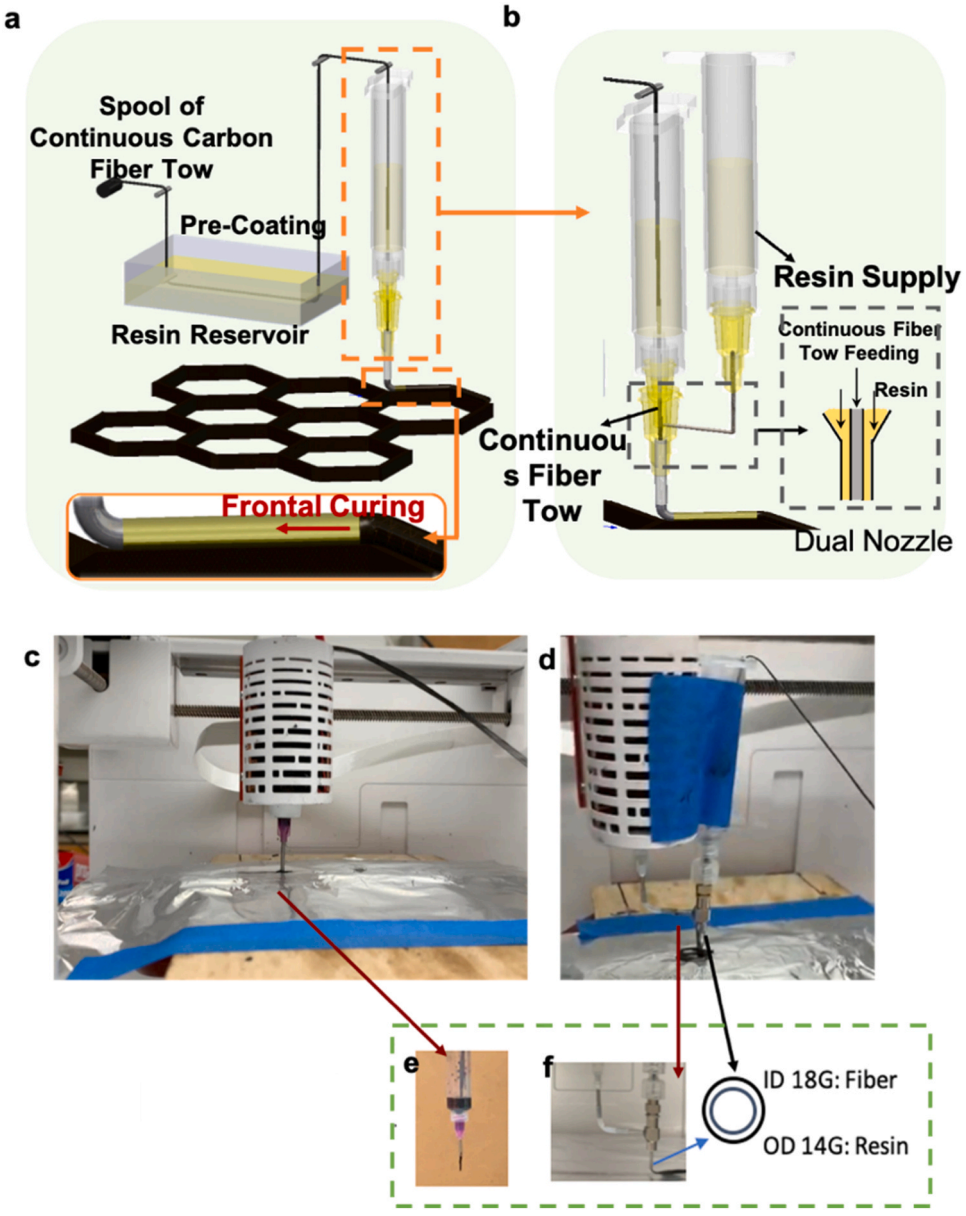

Fig. 1. c-CFTCs printing. a, scheme of c-CFTC single nozzle printing; **b,** scheme of c-CFTC dual nozzle printing; **c**, experiment setup for c-CFTC single nozzle printing; **d**, experiment setup for c-CFTC dual nozzle printing; **e,** enlarged single nozzle; **f,** enlarged dual nozzle.

to obtain a good accuracy of filament deposition during printing due to the nature of fiber tow flexibility. To increase the fiber volume fraction and achieves freestanding composites structure in 3D spaces, dual extrusion processes were also designed and introduced for c-CFTC printing.

In dual nozzle extrusion captured in Fig. 1d and f, fiber tow was threaded into the inner print head while the resin was supplied from the outer print head via pneumatic pressure. The coaxial nozzle consists of a 18 G inner nozzle and a 14 G-outer nozzle. The structure of coaxial nozzle and its printing mechanism is shown in the dashed grey box in Fig. 1b. As illustrated by the figure, the coaxial nozzle has two channels, an inner channel which feeds the continuous fiber tow and an outer channel that supplies the reactive resin. With such a dual nozzle structure, the amount of resin in the composites can be controlled and the fiber tow can be ensured to position in the center of the extruded filament for a good accuracy.

The fiber/epoxy resin weight ratio was tuned by incorporating both single and dual nozzle printhead. The fiber volume ratio of the printed c-CFTC was determined following ASTM D3171. Specifically, the specimen mass was measured and then the matrix portion of this specimen was removed in furnace via pyrolysis. The remaining fiber content was measured, and the weight percent of fiber was calculated. The volume percent was determined according to the nominal densities of both matrix and fibers.

2.8. Mechanical property testing

The cuboid c-CFTC specimens with 15 × 6 × 3 mm according to ASTM D3039 were printed with different fiber/epoxy volume ratios for tensile testing in a tensile machine (MTS Insight) with a 30 kN load cell. Tabs are attached on both sides to protect the specimens during the tensile test. A constant crosshead speed of 2 mm/min was set for the tensile test. Extensometer was used for recording the displacement for strain and Young's modulus calculation. Young's modulus is calculated within the strain range of 0.02–0.12%. The sample preparation and subsequent flexural strength measurement were based on the ASTM D7264. Specifically, the diameter of the loading rod was tuned to 5 mm, and the loading speed was set to 2 mm/min.

3. Results and discussion

3.1. Frontal curing behavior

The resin soaked on the fiber tows should be sufficient to sustain frontal reaction, and thus highly exothermic epoxy resin and efficient initiation process are critical to minimize the resin amount in the tows. The key to ensure the sustainable frontal propagation lies in the ink formulation, and the initiation process is the vital step for the curing reaction. A series of initiating systems were studied for BADGE frontal curing. The molecular structure of BADGE is shown in Fig. S1. The reported frontal propagation behaviors are summarized in Fig. 2a and Note 1, and the corresponding reactivities are shown in Fig. 2b. BADGE epoxy resin shows a lower reactivity and is harder to achieve a sustainable frontal reaction in comparison to the DCPD resin. DCPD with Grubb catalyst shows a steep reaction profile (Fig. 1d), which means that a thrust of energy releases at the activation temperature. The rapid reaction and sudden energy release enable the high propagation rate. In contrast, a flat heat flow is observed for BADGE with amine catalyst, indicating that curing progresses at a lower reaction rate. As a result, amine/BADGE could not achieve a sustainable frontal curing. Compared to DCPD with GC2 catalyst reaction system (yellow square), most previous BADGE systems exhibited lower production rates. For the I-Al/I-TI initiating systems, it exhibited a high propagation rate at a propagation temperature. The high reaction temperature may cause over-curing with a second or third exothermic reaction peak as well as potential degradation. The resin color changed from transparent to black, indicating an overheating issue (inset image i and ii in Fig. 2b). To avoid the high propagation temperature, the curing reaction needs to be tailored for meeting the printing requirement.

3.2. Resin formulations

Before fiber impregnation, ink formulations were studied to tune the frontal propagation behavior. The effects of I-TI and I-Al on BADGE frontal curing reaction were studied, respectively. Their effects on the frontal reaction kinetics were analyzed through DSC and the results are shown in Fig. 3a and b. When the I-TI: I-Al ratio was at 2 mol%: 1 mol%, the peak reaction temperature was found to be 125.5 °C (1st peak) while enthalpy was calculated to be 488.82 J g^{-1}. At a decreasing I-Al concentration (I-TI remains), the peak reaction temperature and enthalpy both went down. Particularly, when I-Al concentration dropped from

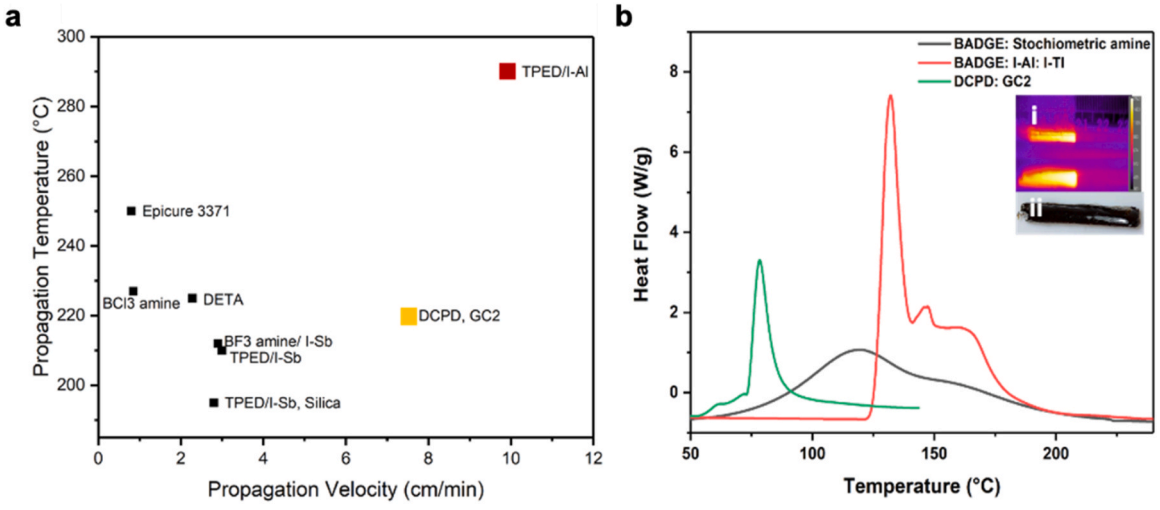

Fig. 2. Frontal Reaction Overview. a, comparison of front temperature and front velocity of the current initiating system to previously reported BADGE epoxy resin (black and red square) and DCPD systems (yellow square) [1,27,35–38,40,41]; **b**: reaction profile of DCPD with Grubb catalyst (green), BADGE with amine catalyst (black) and current I-Al: I-TI initiating system (I-Al: I-TI −2 mol%: 2 mol%) (red); inset image: i, infrared (IR) image analysis of epoxy resin front propagation; ii, picture of the frontal cured part (bulk, dark and opaque).

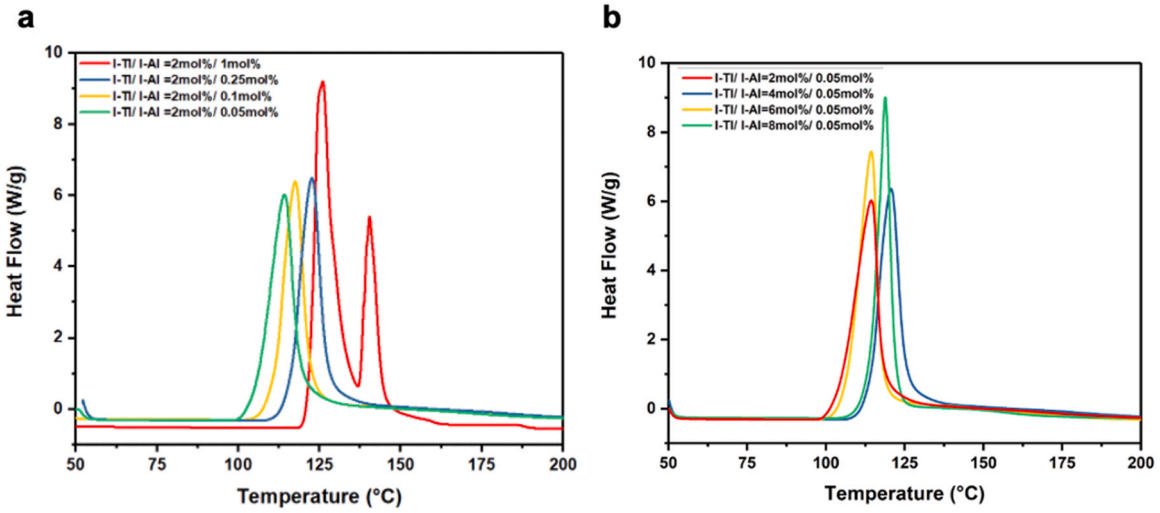

Fig. 3. Reaction profiles (DSC) for varying a, I-Al; b, I-TI concentrations.

1 mol% to 0.1 mol%, the peak reaction temperature dropped 8 °C and the peak heat flow dropped from 9.2 to 6.38 W g^{-1} while the enthalpy remained. Further reduction of the I-Al concentration from 0.1 mol% to 0.05 mol% led to a decrease of the peak reaction temperature to 114.4 °C and the peak heat flow was slightly reduced to 6.03 W g^{-1}. Details of peak reaction temperature, peak heat flow, and the enthalpy are shown in Table S1. The reaction rate at each initiator concentration was also determined by the DSC results, as shown in Fig. S2. Resins with 1 mol% I-Al showed a significantly higher reaction rate compared to resins with a lower I-Al concentration. At low I-Al concentrations, the reaction rate was lowered due to the limited number of Lewis acid formed from I-Al nucleophiles, which further limited the number of protons attacking the epoxide for ring-opening reaction, as shown in Fig. 4. In contrast, there was no such obvious trend in reducing the peak reaction temperature and increasing reaction rate at an increasing I-TI concentration, as shown in Fig. 3b, Fig. S2b, and Table S1. However, at higher I-TI concentrations (6 mol% and 8 mol%), the reaction enthalpy decreased ~10 J g^{-1}. This may indicate an incomplete cure for parts at higher I-TI concentrations due to the large mismatch in I-TI and I-Al concentrations. The phenomenon observed for different I-TI concentrations can be explained by the reaction mechanism of the radical-induced cationic frontal reaction, shown in Fig. 4. In the reaction, the thermal labile bond in I-TI was broken by local heat and generated radicals. Subsequently, the radicals from I-TI induce Lewis acid by interacting with nucleophiles from I-Al for epoxide ring-opening reaction. As a result, the increasing number of radicals could greatly surpass other reactive species, and the reaction rate depends on the nucleophiles from I-Al.

The frontal propagation behavior can be characterized with front velocity (V_f), the distance that a frontal region could transport in unit time, and frontal temperature (T_f), the temperature of the reaction front. V_f and T_f are the two key parameters for the frontal reaction that determines the rate of production and the performance of as-printed structures. A high-resolution forward-looking infrared (FLIR) camera was employed for in-situ monitoring of the frontal reaction (V_f and T_f) and the calculation results are shown in Fig. 2d, e. (The detailed description of the calculation, the measurement set up, and IR camera calibration are provided in Figs. S3–4 and Note 2). V_f and T_f were observed to go up with the increasing I-Al concentration from 0.02 mol % to 2 mol% when I-TI remained constant (2 mol%), as shown in Fig. 5a, indicating a significant effect of I-Al in tuning the reaction kinetics. In contrast, V_f and T_f only slightly increased from 237 °C to 241 °C when I-TI concentrations increased from 2 mol% to 8 mol%, much less significant in tuning the reaction rate compared to I-Al, as shown in Fig. 5b. This phenomenon coincides with the measured reaction profile shown in Fig. 3b, indicating that I-Al is more critical to the reaction rate and reaction temperature. The reaction rate and frontal temperature were tuned with varying initiator concentrations. The part cured at higher temperatures turned into darker color (inset image i in Fig. 5a) compared to the one cured at a lower temperature (inset image ii in Fig. 2d), indicating potential degradation. This is further verified by TGA where noticeable weight loss was observed when the curing temperature reached 260 °C (Fig. S5 and Note 3). Based on the analysis, 4 mol% I-TI and 0.05 mol% I-Al incorporated epoxy resins were selected for the further study.

3.3. c-CFTCs printing and front propagation analysis

The self-sustaining in-situ curing enables the construction of

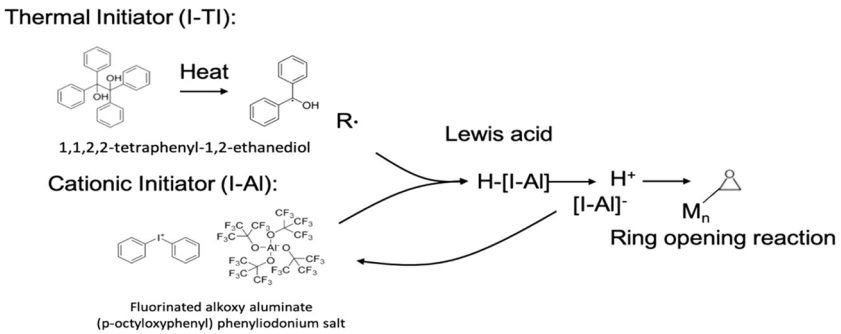

Fig. 4. Epoxy resin frontal curing reaction mechanism.

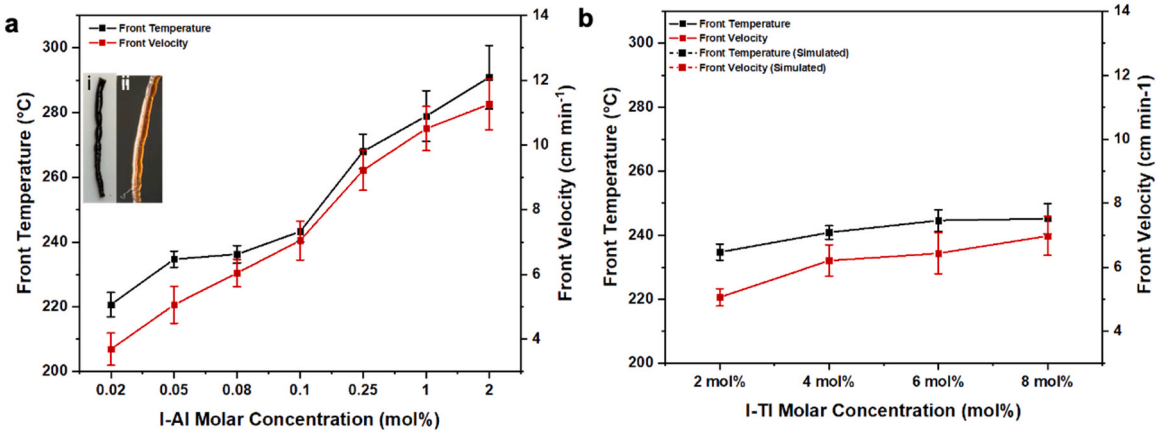

Fig. 5. Effect of **d**, I-Al, **e**, I-TI concentration on front temperature and front velocity.

freestanding 3D composites and significantly reduces the energy consumption by eliminating the secondary curing process. Highly thermal conductive carbon fiber serves as a good medium for exothermic energy transportation, dissipation, and re-distribution, improves the exothermic energy utilization, and minimizes the energy loss to the environment. The challenge of achieving exceptional mechanical performance of as-printed c-CFTCs lies in tuning the resin amount for ensuring a high fiber volume fraction and also a decent self-sustaining in-situ curing. The epoxy resin-based inks containing I-Al/I-TI initiating system were loaded into the resin reservoir. The resin volume was tuned by using a printhead with different gauges as well as the co-axial printhead. Fiber tow threaded through the inner printhead while the inks were injected from the outer printhead to assure the fiber tow stayed in the center of the printed filament. Subsequently, epoxy resin-based c-CFTCs printing was demonstrated, as shown in Fig. 6a, b. The free-standing spiral structures were printed since epoxy resins instantaneously crosslinked into polymer network upon extrusion which was synchronized with the reactive front. The part in Fig. 6a was printed using single nozzle while the part in Fig. 6b was printed using dual nozzle setup.

The nozzle deposition speed was synchronized with the velocity of the reaction front to assure the continuous free-form printing. The front propagation behavior of epoxy resin was analyzed with the presence of continuous carbon fibers and the results are shown in Fig. 6c. The V_f and T_f were measured using the same method for neat resins. With the inclusion of highly thermal conductive fiber tows, thermal diffusion along the fiber direction is improved. This helps to preheat the resins ahead of the frontal reaction zone, resulted in a higher V_f. Here, printheads with 800 μm diameter (18 gauge) and 1630 μm diameter (14 gauge) were used for c-CFTC printing, resulting in the printed parts with the fiber volume ratio of 48% and 18%, respectively. For the parts printed with 18 vol% fiber, a higher volume of ink soaked in the fiber tow yields higher V_f and T_f, which may be induced by more thermal energy released from the exothermic reaction. This also caused a slightly higher fontal temperature, as shown in Fig. 6c. With the inclusion of highly thermal conductive fiber tows, thermal diffusion in propagation direction resulted in the front velocity of ~ 7.5 cm/min (48 vol% in fiber) and ~13.8 cm/min (18 vol% in fiber), both higher than that in the neat resin (~6.2 cm/min) (Fig. 6c). For comparison, the neat resin printing results were also provided in Figs. S6-S10, and discussed Note 5 and Note 6. With the measured front velocity, the production rate of the process can be determined. Specifically, the production rate of the continuous carbon fiber composites printing process is calculated to be ~800 cm^3/hour for composites with 18 vol% of fiber based on the printing speed of 13.8 cm/min and ~400 cm^3/hour for composites with 48 vol% of fiber based on the printing speed of 7.5 cm/min.

Numerical simulation was also conducted to reveal the role of continuous carbon fiber tows in thermal transport of epoxy resin frontal curing reaction. The results are shown in Fig. 7. Obviously, the presence of highly thermal conductive continuous carbon fiber enhanced the heat

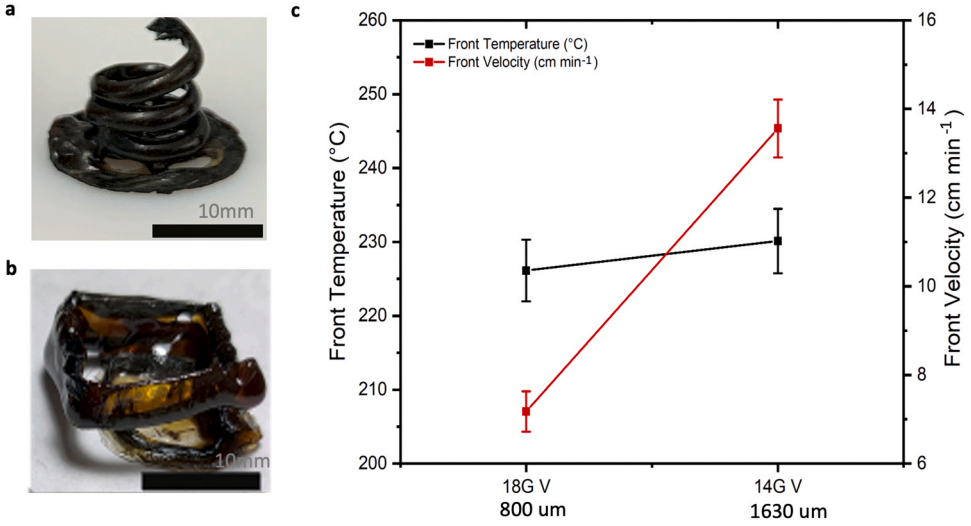

Fig. 6. Frontal reaction enabled c-CFTC printing. a-b, free-standing structure of continuous carbon fiber composites by DIW printing; **c**, front velocity, and front temperature of printing in the vertical direction.

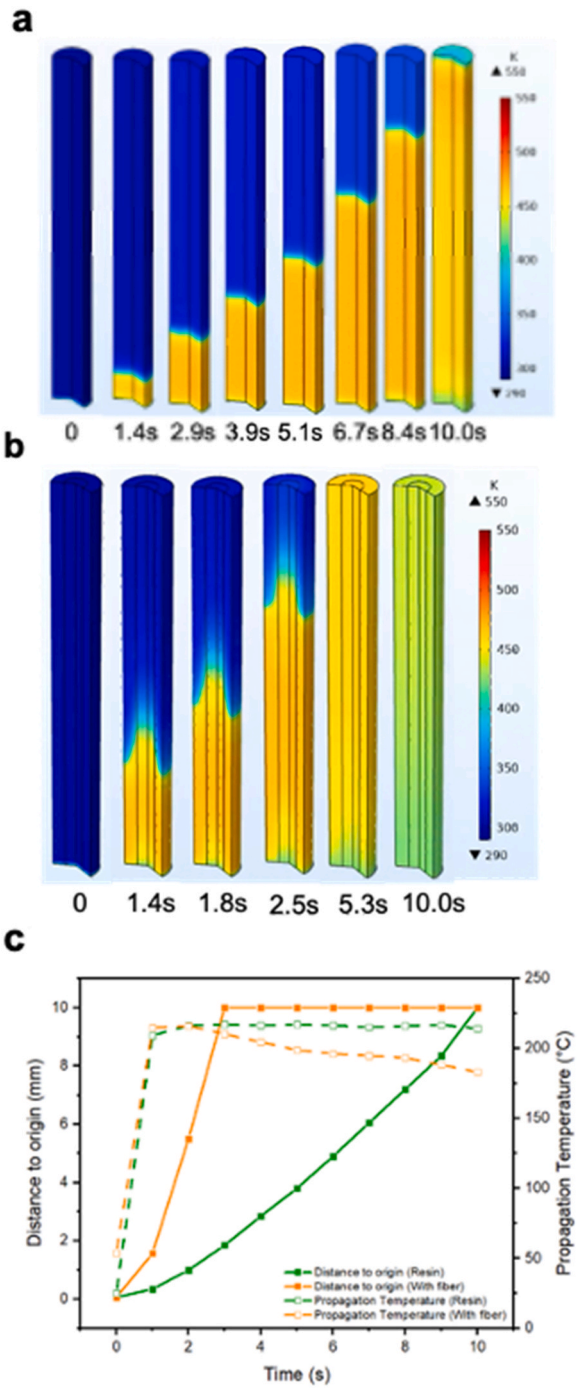

Fig. 7. Numerical simulation. **a**, c-CFTC (0.5 mm diameter fiber rod, 1.12 mm total diameter, length 10 mm) and **b**, neat resin (1 mm diameter rod, length 10 mm); **c**, summarized front propagation velocity and temperature of **a** and **b**. Orange: c-CFTC Green: neat resin. The resins volume kept same for **a** and **b**. The resin's reaction profile used experimental data with I-TI and I-Al concentration of 4 mol%: 0.05 mol%.

transfer in resin's frontal propagation direction, as shown in Fig. 7a and b. The simulation model for continuous fiber/epoxy composites is similar to the one for neat resin except that a strand of continuous carbon fiber tow is positioned in the center of the rod. From the simulation, a sharp temperature gradient was observed due to the large mismatch of thermal conductivities between the carbon-fiber tow and the resin matrix, indicating a more effective thermal transport along and near the continuous fiber surface. This also resulted in a higher propagation rate for the c-CFTC printing, as shown in Fig. 7a and c. Based on the two Partial Differential Equations (PDEs) in Note 4, the thermal diffusion in the surrounding of fiber increased with the presence of highly conductive fiber, resulting in a higher local temperature and thus a higher reaction rate. The detailed propagation results are summarized in Fig. 7c, indicating a higher propagation rate for the fiber incorporated one while the frontal temperature remained.

3.4. Mechanical characterization

Tensile measurements were first conducted on the printed specimens in fiber direction. The c-CFTC tensile specimens were printed using the same printing setup shown in Fig. 1. The tensile properties of as-printed c-CFTCs parts demonstrate exceptional tensile performance that is slightly lower than the traditional resin transfer molding process (~1500 MPa) [42], reaching a tensile strength of ~1147 MPa (Fig. 8a, b). Fiber volume plays an important role in tensile strength. When the fiber fraction was increased from 18 vol% to 48 vol%, the tensile strength was increased from 420 MPa to 1147 MPa.

As-printed c-CFTCs, with 18% fiber volume fraction, showed a higher tensile strength than some continuous CF/thermoplastic composites with 34% fiber volume fraction, as shown in Fig. 9. As-printed c-CFTC (48 vol% fiber fraction) in this paper showed much higher strength than those c-CFTCs fabricated by other methods with 51 – 57 vol% fiber volume reported in literature [1,48] (Fig. 9 and Table S3). The as-printed neat resin with different initiator formulations were printed and tested. The results are shown in Figs. S6–10 and discussed in Note 5 and Note 6. Temperature effect is shown in Fig. S7, and the initiator concentration effect is presented in Fig. S8.

The interlaminar shear strength (ILSS) was also conducted to analyze the mechanical performance of printed specimens when subjected to transverse load. Three-point bend tested was conducted, and the experiment illustration is shown in inset images i and ii in Fig. 10. The ILSS fell within the range of 30–42, which was comparable to the previous reported ILSS value (~40.9 MPa) of continuous carbon fiber composites produced by Yavas et al. [51]. The ILSS results of printed c-CFTC specimens are shown in Fig. 10. Such results indicated that the frontal curing-enabled printing process could lead to competitive mechanical properties.

3.5. Manufacturing efficiency

Oven curing claimed an energy intensity over 10^5 J/cm^3 in the past decades of composite fabrication [2,52]. Such a high energy intensity is mainly caused by the energy-intensive oven and hours curing. Considering the large demand for epoxy resin (market size: USD 8 billion in revenue in 2019 [34] compared to DCPD with a market size of USD 0.86 billion [34]), frontal curing-enabled printing showed a much significant total energy reduction in epoxy resin fabrication (Fig. 11a, Table S4 and Note 7). Different sizes of parts were considered for the energy-saving calculation. The red band in Fig. 11a represents a potential energy saving of printed parts with 50 cm^3 (lower bound) and 2000 cm^3 (upper bound). The dashed lines and red annotations represent the total energy consumption (product of energy intensity and market volume in a year). If this frontal curing-based printing method can be applied to epoxy resins and composites fabrication, potentially 1.3×10^{10} MJ/year of energy (3.6 billion kilowatt-hours/year) can be reduced while only 10% of the amount of energy can be reduced for applying frontal polymerization-based DCPD printing (Fig. 11a blue lines and Table S4). The frontal curing-based printing of epoxy resins represents an energy intensity six orders of magnitudes lower than the conventional oven curing process in fabricating a large piece (2000 cm^3) (Fig. 11b). Besides, specimens printed via frontal polymerization showed comparable tensile strength to other reported additive manufacturing methods but consumed much less energy (~4 orders of magnitude lower, as shown in Fig. 11b, Table S5–6 and explained in Note 7 and Note 8).

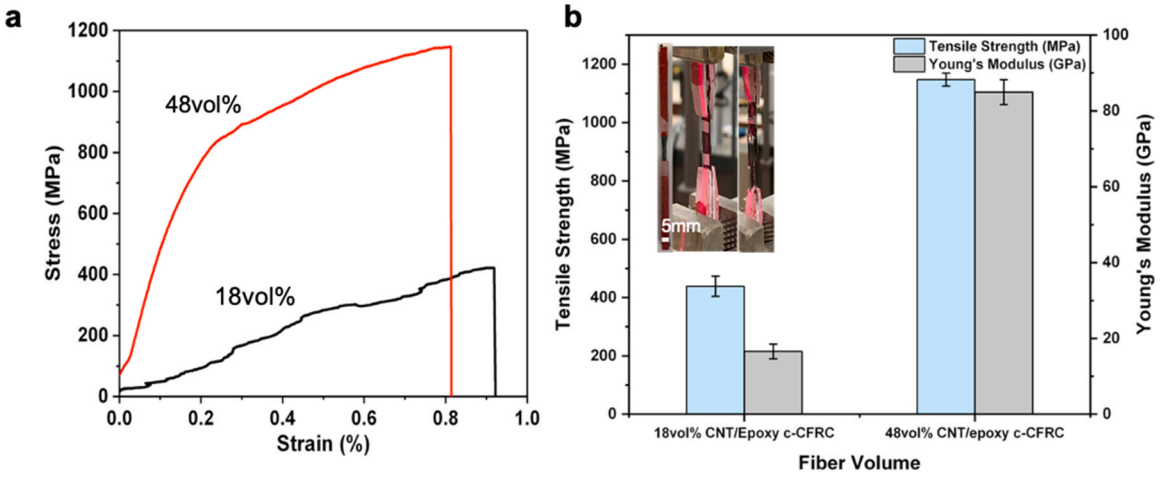

Fig. 8. Tensile Performance. a, plot of the original stress-strain curve of c-CFTC tensile bars tensile strength, and Young's modulus of epoxy resin/c-CFTC with 18 and 48 fiber volume; **b,** c-CFTC tensile bars tensile strength, and Young's modulus of epoxy resin/c-CFTC with 18 and 48 fiber volume. Inset images are the printed c-CFTC specimens for tensile test and the specimen loaded for tensile testing with a laser extensometer, demonstration of printed tensile bars and pulling process.

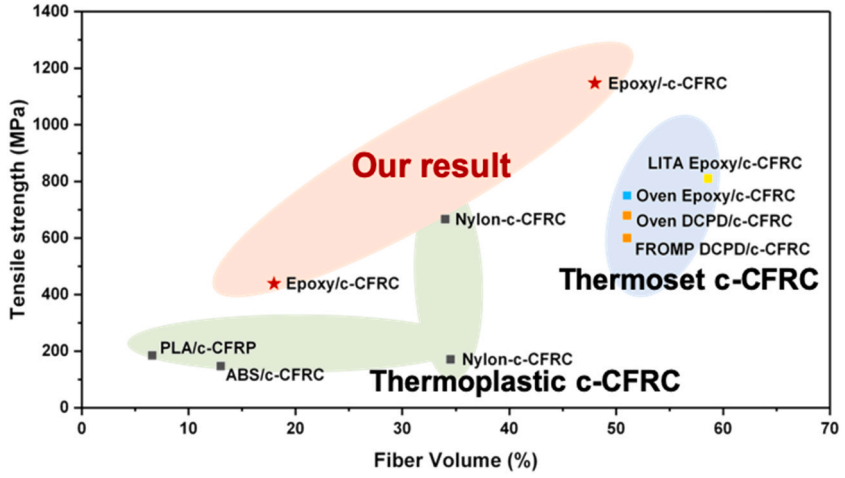

Fig. 9. Comparison of tensile strength and Young's Modulus of fabricated specimens with other representative additive manufacturing methods [1,17,43–50] (our results are presented in star symbol and previous reports are noted in square symbol).

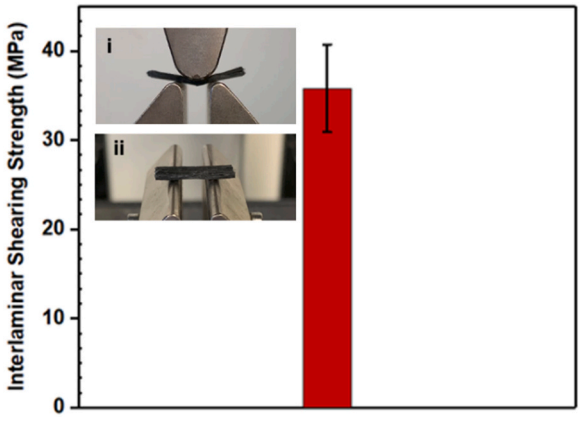

Fig. 10. Flexural Testing of continuous carbon fiber composites. Inset images are the illustration of three-point bend test.

4. Conclusion

A rapid and energy-efficient print-and in-situ cure of aerospace-grade epoxy resin-based c-CFTC have been demonstrated. Reducing the I-Al concentration can effectively decrease the front reaction temperature while I-TI is less effective in tuning the front propagation behavior. The continuous carbon fiber tows were soaked in frontal curable resins to print c-CFTCs, and the frontal velocity can range from 7 to 14 cm/min dependent on the resin volume fractions while the frontal temperature stayed flat at ~230 °C. As-printed c-CFTCs exhibited a tensile strength of ~1.147 GPa at a 48 vol% fiber fraction, and it is comparable to previous oven-cured thermosets-based c-CFTCs but this method consumes 4 orders of magnitudes less energy. Further projection of this method into industrial production indicated that fabricating epoxy resin-based c-CFTCs with this frontal curing method could potentially save 3.6 billion kilowatt-hours of energy per year.

CRediT authorship contribution statement

Zimeng Zhang: Investigation, Data curation; Formal analysis, Validation, Project administration, Writing – original draft, Writing – review & editing. **Ruochen Liu:** Investigation, Data curation; Formal analysis;

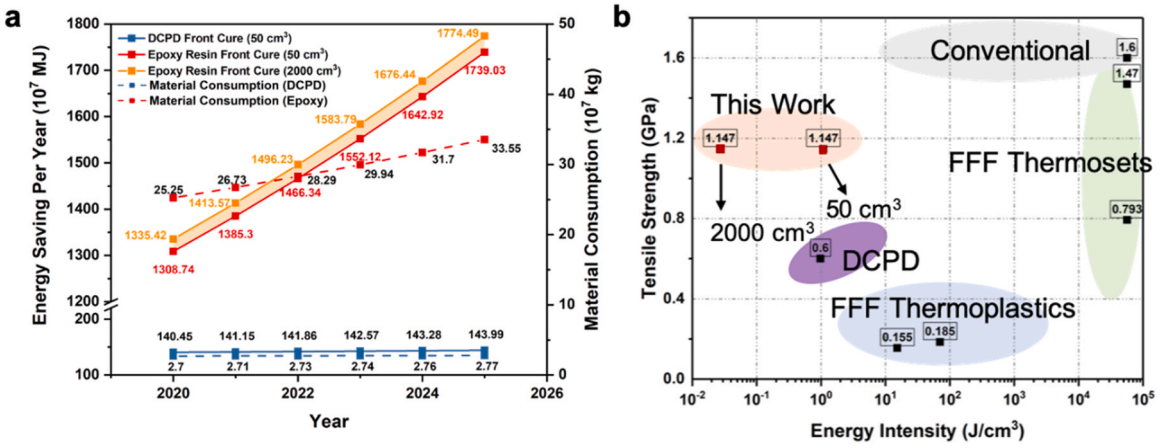

Fig. 11. Production efficiency calculation and comparison to other reported continuous CFTCs printing methods. a, energy saving and material consumption over the years (2020–2025) [1]. **b**, Comparison of tensile performance of continuous CFTC versus energy intensity. Frontally cured continuous CFTC exhibited equivalent or higher tensile strength than other reported methods including both thermoplastics and thermosets-based c-CFTC fabrication [2,17,43,44,47]. (FFF: fused filament deposition with oven post curing).

Validation, Writing – review & editing. **Yuchen Liu**: Investigation. **Wei Li**: Investigation. **Haochen Luo**: Data curation; Formal analysis. **Li Zeng:** Resources, Writing – review & editing. **Jingjing Qiu**: Funding Acquisition, Writing – review & editing. **Shiren Wang**: Conceptualization, Funding Acquisition, Methodology, Supervision, Writing – review & editing.

Declaration of Competing Interest

The authors declare that they have no known competing financial interests or personal relationships that could have appeared to influence the work reported in this paper.

Acknowledgments

This work is supported by the National Science Foundation (CMMI-1934120, CMMI-1933679).

Appendix A. Supporting information

Supplementary data associated with this article can be found in the online version at doi:10.1016/j.addma.2021.102348.

References

[1] I.D. Robertson, M. Yourdkhani, P.J. Centellas, J.E. Aw, D.G. Ivanoff, E. Goli, E. M. Lloyd, L.M. Dean, N.R. Sottos, P.H. Geubelle, J.S. Moore, S.R. White, Rapid energy-efficient manufacturing of polymers and composites via frontal polymerization, Nature 557 (7704) (2018) 223–227.
[2] J.V. Anguita, C.T.G. Smith, T. Stute, M. Funke, M. Delkowski, S.R.P. Silva, Dimensionally and environmentally ultra-stable polymer composites reinforced with carbon fibres, Nat. Mater. 19 (3) (2020) 317–322.
[3] E. Mazzon, A. Habas-Ulloa, J.-P. Habas, Lightweight rigid foams from highly reactive epoxy resins derived from vegetable oil for automotive applications, Eur. Polym. J. 68 (2015) 546–557.
[4] W. Han, S. Chen, J. Campbell, X. Zhang, Y. Tang, Fracture toughness and wear properties of nanosilica/epoxy composites under marine environment, Mater. Chem. Phys. 177 (2016) 147–155.
[5] M. Janvier, L. Hollande, A.S. Jaufurally, M. Pernes, R. Ménard, M. Grimaldi, J. Beaugrand, P. Balaguer, P.H. Ducrot, F. Allais, Syringaresinol: a renewable and safer alternative to bisphenol A for epoxy-amine resins, ChemSusChem 10 (4) (2017) 738–746.
[6] M. Martí, E. Armelin, J.I. Iribarren, C. Alemán, Soluble polythiophenes as anticorrosive additives for marine epoxy paints, Mater. Corros. 66 (1) (2015) 23–30.
[7] J. Chen, A. Lekawa-Raus, J. Trevarthen, T. Gizewski, D. Lukawski, K. Hazra, S. S. Rahatekar, K.K.K. Koziol, Carbon nanotube films spun from a gas phase reactor for manufacturing carbon nanotube film/carbon fibre epoxy hybrid composites for electrical applications, Carbon 158 (2020) 282–290.
[8] Z. Chen, B. Chisholm, J. Kim, S. Stafslien, R. Wagner, S. Patel, J. Daniels, L.V. Wal, J. Li, K. Ward, UV-curable, oxetane-toughened epoxy-siloxane coatings for marine fouling-release coating applications, Polym. Int. 57 (6) (2008) 879–886.
[9] C. Dong, H.A. Ranaweera-Jayawardena, I.J. Davies, Flexural properties of hybrid composites reinforced by S-2 glass and T700S carbon fibres, Compos. Part B: Eng. 43 (2) (2012) 573–581.
[10] M. Quanjin, M.R.M. Rejab, J. Kaige, M.S. Idris, M.N. Harith, Filament winding technique, experiment and simulation analysis on tubular structure, IOP Conf. Ser.: Mater. Sci. Eng. 342 (1) (2018), 012029.
[11] M.R. Abusrea, S.W. Han, K. Arakawa, N.S. Choi, Bending strength of CFRP laminated adhesive joints fabricated by vacuum-assisted resin transfer molding, Compos. Part B: Eng. 156 (2019) 8–16.
[12] J.P. Pascault, R.J.J. Williams, Overview of thermosets: present and future, Thermosets (2018) 3–34.
[13] B. Shi, Y. Shang, P. Zhang, A.P. Cuadros, J. Qu, B. Sun, B. Gu, T.-W. Chou, K.K. Fu, Dynamic capillary-driven additive manufacturing of continuous carbon fiber composite, Matter 2 (6) (2020) 1594–1604.
[14] B.G. Compton, J.A. Lewis, 3D-printing of lightweight cellular composites, Adv. Mater. 26 (34) (2014) 5930–5935.
[15] M. Hegde, V. Meenakshisundaram, N. Chartrain, S. Sekhar, D. Tafti, C.B. Williams, T.E. Long, 3D printing all-aromatic polyimides using mask-projection stereolithography: processing the nonprocessable, Adv. Mater. (Deerfield Beach, Fla.) 29 (31) (2017), 1701240.
[16] B. Wang, Z. Zhang, Z. Pei, J. Qiu, S. Wang, Current progress on the 3D printing of thermosets, Adv. Compos. Hybrid. Mater. 3 (2020) 1–7.
[17] Y. Ming, Y. Duan, B. Wang, H. Xiao, X. Zhang, A novel route to fabricate high-performance 3D printed continuous fiber-reinforced thermosetting polymer composites, Materials 12 (9) (2019) 1369.
[18] Z. Zhang, B. Wang, D. Hui, J. Qiu, S. Wang, 3D bioprinting of soft materials-based regenerative vascular structures and tissues, Compos. Part B: Eng. 123 (2017) 279–291.
[19] M.B.A. Tamez, I. Taha, A review of additive manufacturing technologies and markets for thermosetting resins and their potential for carbon fiber integration, Addit. Manuf. (2020), 101748.
[20] D. Lei, Y. Yang, Z. Liu, S. Chen, B. Song, A. Shen, B. Yang, S. Li, Z. Yuan, Q. Qi, A general strategy of 3D printing thermosets for diverse applications, Mater. Horiz. 6 (2) (2019) 394–404.
[21] B. Wang, K.F. Arias, Z. Zhang, Y. Liu, Z. Jiang, H.-J. Sue, N. Currie-Gregg, S. Bouslog, Z.Z.J. Pei, S. Wang, 3D printing of in-situ curing thermally insulated thermosets, Manuf. Lett. 21 (2019) 1–6.
[22] B.G. Compton, J.A. Lewis, 3D-printing of lightweight cellular composites, Adv. Mater. 26 (34) (2014) 5930–5935.
[23] B. Wang, Y. Ming, Y. Zhu, X. Yao, G. Ziegmann, H. Xiao, X. Zhang, J. Zhang, Y. Duan, J. Sun, Fabrication of continuous carbon fiber mesh for lightning protection of large-scale wind-turbine blade by electron beam cured printing, Addit. Manuf. 31 (2020), 100967.
[24] P. Parandoush, C. Zhou, D. Lin, Laser additive manufacturing bulk graphene-copper nanocomposites, Nanotechnology 28 (2) (2017), 445705.
[25] X. He, Y. Ding, Z. Lei, S. Welch, W. Zhang, M. Dunn, K. Yu, 3D printing of continuous fiber-reinforced thermoset composites, Addit. Manuf. 40 (2021), 101921.
[26] Q. Shi, K. Yu, X. Kuang, X. Mu, C.K. Dunn, M.L. Dunn, T. Wang, H.J. Qi, Recyclable 3D printing of vitrimer epoxy, Mater. Horiz. 4 (4) (2017) 598–607.
[27] J.A. Pojman, V.M. Ilyashenko, A.M. Khan, Free-radical frontal polymerization: self-propagating thermal reaction waves, J. Chem. Soc. Faraday Trans. 92 (16) (1996) 2825–2837.

[28] I.D. Robertson, E.L. Pruitt, J.S. Moore, Frontal ring-opening metathesis polymerization of exo-dicyclopentadiene for low catalyst loadings, ACS Macro Lett. 5 (5) (2016) 593–596.
[29] A. Mariani, S. Fiori, Y. Chekanov, J.A. Pojman, Frontal ring-opening metathesis polymerization of dicyclopentadiene, Macromolecules 34 (19) (2001) 6539–6541.
[30] A. Ruiu, D. Sanna, V. Alzari, D. Nuvoli, A. Mariani, Advances in the frontal ring opening metathesis polymerization of dicyclopentadiene, J. Polym. Sci. Part A: Polym. Chem. 52 (19) (2014) 2776–2780.
[31] I.D. Robertson, L.M. Dean, G.E. Rudebusch, N.R. Sottos, S.R. White, J.S. Moore, Alkyl phosphite inhibitors for frontal ring-opening metathesis polymerization greatly increase pot life, ACS Macro Lett. 6 (6) (2017) 609–612.
[32] R. Thomas, D. Yumei, H. Yuelong, Y. Le, P. Moldenaers, Y. Weimin, T. Czigany, S. Thomas, Miscibility, morphology, thermal, and mechanical properties of a DGEBA based epoxy resin toughened with a liquid rubber, Polymer 49 (1) (2008) 278–294.
[33] S. Han, Q. Meng, Z. Qiu, A. Osman, R. Cai, Y. Yu, T. Liu, S. Araby, Mechanical, toughness and thermal properties of 2D material-reinforced epoxy composites, Polymer 184 (2019), 121884.
[34] Plastic Market Size, Share & Trends Analysis Report By Product (PE, PP, PU, PVC, PET, Polystyrene, ABS, PBT, PPO, Epoxy Polymers, LCP, PC, Polyamide), By Application, By Region, And Segment Forecasts, 2020 - 2027; 2020.
[35] A. Mariani, S. Bidali, S. Fiori, M. Sangermano, G. Malucelli, R. Bongiovanni, A. Priola, UV-ignited frontal polymerization of an epoxy resin, J. Polym. Sci. Part A: Polym. Chem. 42 (9) (2004) 2066–2072.
[36] D. Bomze, P. Knaack, R. Liska, Successful radical induced cationic frontal polymerization of epoxy-based monomers by C–C labile compounds, Polym. Chem. 6 (47) (2015) 8161–8167.
[37] A.D. Tran, T. Koch, P. Knaack, R. Liska, Radical induced cationic frontal polymerization for preparation of epoxy composites, Compos. Part A: Appl. Sci. Manuf. 132 (2020), 105855.
[38] P. Knaack, N. Klikovits, A.D. Tran, D. Bomze, R. Liska, Radical induced cationic frontal polymerization in thin layers, J. Polym. Sci. Part A: Polym. Chem. 57 (11) (2019) 1155–1159.
[39] O. Uitz, P. Koirala, M. Tehrani, C.C. Seepersad, Fast, low-energy additive manufacturing of isotropic parts via reactive extrusion, Addit. Manuf. 41 (2021), 101919.
[40] Arutiunian, K.A.; Davtyan, S.P.; Rozenberg, B.A.; Enikolopyan, N.S. In Curing of epoxy resins of bis-phenol a by amines under conditions of reaction front propagation, 1975; pp 657–660.
[41] Surkov, N.F.; Davtyan, S.P.; Rozenberg, B.A.; Enikolopyan, N.S. In Calculation of the steady velocity of the reaction front during hardening of epoxy oligomers by diamines, 1976; pp 435–438.
[42] D.D.L. Chung, Processing-structure-property relationships of continuous carbon fiber polymer-matrix composites, Mater. Sci. Eng.: R: Rep. 113 (2017) 1–29.
[43] W. Hao, Y. Liu, H. Zhou, H. Chen, D. Fang, Preparation and characterization of 3D printed continuous carbon fiber reinforced thermosetting composites, Polym. Test. 65 (2018) 29–34.
[44] R. Matsuzaki, M. Ueda, M. Namiki, T.-K. Jeong, H. Asahara, K. Horiguchi, T. Nakamura, A. Todoroki, Y. Hirano, Three-dimensional printing of continuous-fiber composites by in-nozzle impregnation, Sci. Rep. 6 (2016) 23058.
[45] B. Shi, Y. Shang, P. Zhang, A.P. Cuadros, J. Qu, B. Sun, B. Gu, T.-W. Chou, K. Fu, Dynamic capillary-driven additive manufacturing of continuous carbon fiber composite, Matter 2 (6) (2020) 1594–1604.
[46] X. Tian, T. Liu, Q. Wang, A. Dilmurat, D. Li, G. Ziegmann, Recycling and remanufacturing of 3D printed continuous carbon fiber reinforced PLA composites, J. Clean. Prod. 142 (2017) 1609–1618.
[47] X. Tian, T. Liu, C. Yang, Q. Wang, D. Li, Interface and performance of 3D printed continuous carbon fiber reinforced PLA composites, Compos. Part A: Appl. Sci. Manuf. 88 (2016) 198–205.
[48] N. van de Werken, J. Hurley, P. Khanbolouki, A.N. Sarvestani, A.Y. Tamijani, M. Tehrani, Design considerations and modeling of fiber reinforced 3D printed parts, Compos. Part B: Eng. 160 (2019) 684–692.
[49] F. Van Der Klift, Y. Koga, A. Todoroki, M. Ueda, Y. Hirano, R. Matsuzaki, 3D printing of continuous carbon fibre reinforced thermo-plastic (CFRTP) tensile test specimens, Open J. Compos. Mater. 06 (01) (2016) 18–27.
[50] C. Yang, X. Tian, T. Liu, Y. Cao, D. Li, 3D printing for continuous fiber reinforced thermoplastic composites: mechanism and performance, Rapid Prototyp. J. 23 (2017) 209–215.
[51] D. Yavas, Z. Zhang, Q. Liu, D. Wu, Interlaminar shear behavior of continuous and short carbon fiber reinforced polymer composites fabricated by additive manufacturing, Compos. Part B: Eng. 204 (2021), 108460.
[52] Deborah A. Sunter, W.R. M.I., Joseph W. Cresko, Heather P.H. Liddell, The manufacturing energy intensity of carbon fiber reinforced polymer composites and its effect on life cycle energy use for vehicle door lightweighting. 20th International Conference on Composite Materials 2015, Copenhagen.